Jurnal Teknologi

NUMERICAL STUDY ON EFFECT OF PHASE ANGLE ON TORSIONAL AND LATERAL VIBRATIONS IN POWER TRANSMISSION SYSTEM EMPLOYING CARDAN SHAFT

Mohd Hazri Omar[a]*, Muhajir Ab Rahim[b], Mohd Noor Arib Md Rejab[a]

[a]Faculty of Mechanical Engineering and Technology, UNIMAP, 02600, Arau, Perlis, Malaysia
[b]Faculty of Electrical Engineering and Technology, UNIMAP, 02600, Arau, Perlis, Malaysia

*Corresponding author
muhajir@unimap.edu.my

Graphical abstract
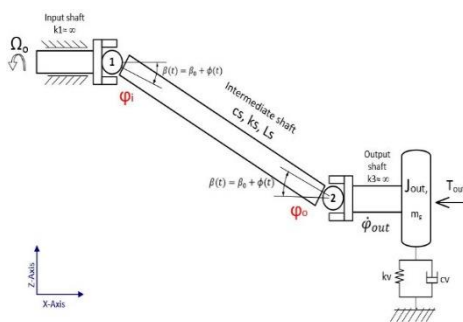
Abstract

A power transmission system driven by a Cardan shaft may experience severe vibration due to fluctuating rotational speed and moments transferred to the final drives, determined by the level of angular misalignment and phasing of the joint yokes. This study investigates the potential of an out-of-phase position displaced by a phase angle in attenuating vibrations. The governing equations representing the dynamics of the system are derived. The torsional and lateral vibration responses are numerically calculated over a range of input rotational speeds. When attenuating the vibration, the phase angle is set equal to the maximum twist that occurs during the in-phase position. Relative attenuation is used to investigate the phase angle effects. The effectiveness is studied for different levels of static angular misalignment. For the considered system, the results showed that for static angular misalignment greater than 20 degrees, the proposed phase angle arrangement could attenuate torsional vibration by more than 10 percent and significantly attenuate the lateral vibration.

Keywords: Cardan shaft, torsional vibration, lateral vibration, phase angle, relative attenuation

Abstrak

Sistem penghantaran kuasa yang didorong oleh aci Cardan mungkin mengalami getaran yang teruk disebabkan oleh kelajuan putaran yang berubah-ubah dan momen yang dipindahkan ke pemacu akhir, ditentukan oleh tahap sudut jajaran dan fasa sendi. Kajian ini menyiasat potensi kedudukan luar fasa yang disesarkan oleh sudut fasa dalam mengurangkan getaran. Persamaan gerakan yang mewakili dinamik sistem diterbitkan. Tindak balas getaran kilasan dan sisi dikira secara berangka pada julat kelajuan putaran input. Dalam melemahkan getaran, sudut fasa ditetapkan sama dengan putaran maksimum yang berlaku semasa kedudukan dalam fasa. Pengecilan relatif digunakan untuk menyiasat kesan sudut fasa. Keberkesanan dikaji untuk pelbagai tahap ketidakjajaran sudut statik. Bagi sistem yang dipertimbangkan, keputusan menunjukkan bahawa untuk sudut jajaran statik lebih daripada 20 darjah, susunan sudut fasa yang dicadangkan boleh melemahkan getaran kilasan lebih daripada 10 peratus dan melemahkan getaran sisi dengan ketara.

Kata kunci: Aci Cardan, getaran kilasan, getaran sisi, sudut fasa, pengecilan relatif

1.0 INTRODUCTION

The Cardan shaft is a critical power transmission component in modern rotational machinery and has been utilized in a wide range of systems such as automobiles, agricultural, and rail vehicles [1–4]. It is equipped with a universal joint at both ends to accommodate either parallel or angular misalignment between the driving and driven sides. However, the Cardan shaft causes a potential vibration problem due to the kinematics of the universal joint. The joint generates both torsional and lateral vibrations [5, 6]. The vibrations are dynamically coupled and are determined by system geometry, which includes the degree of angular misalignment and the phasing of the joint yokes. It has been demonstrated that the rotation of the misaligned Cardan shaft caused an unbalanced force to act on transmission components, failing the gearbox and the cause of fracture of connecting bolts installed in the high-speed train [7, 8]. In numerous applications, the geometry is varied due to operating conditions. So, determining the impact of changes in system geometry especially phase angle, on system vibration is an essential and practical task.

Many studies have been conducted on the dynamics of transmission systems driven by a single universal joint, such as torsional vibration [9, 10] and lateral vibration [11, 12]. DeSmidt et al. [13] investigate the interaction of the lateral and torsional dynamics of a rotor disc system mounted on a soft support condition while being driven through a universal joint. The stability of the system with different levels of angular misalignment has been analysed using the Floquet theory. Results showed that the angular misalignment induced dynamic coupling between lateral and torsion vibrations. The coupled could lead to parametric instability close to sum-type combinations of lateral and torsional natural frequencies. Xia et al. [14, 15] conducted a numerical and experimental study on the coupled torsion-lateral vibration of a 4WD driveline system. The universal joint produced an external excitation force in a lateral direction. The torsional and lateral vibrations were excited when twice input rotational speed equals each of the torsional and lateral natural frequencies. In controlling the second-order vibration, the universal joint was replaced with a flexible coupling, significantly reducing the second-order vibration. Tchomeni et al. [16] studied the dynamic characteristics of two misaligned rotors connected by universal joint under the influences of unbalance rotor condition. The vibration induced by the combination of misalignment and unbalance is characterised by a frequency component which is two times the running speed. Later, Tchomeni and Alugongo [17] conducted theoretical and experimental analysis of a coupled lateral and torsional vibrations of the rotor system under the influences of unbalance rotor and cracked shaft. Crack characteristics are revealed by the appearance of super-harmonic excitation in the frequency spectrum.

Regarding the dynamic of power transmission systems driven by the Cardan shaft, Browne and Palazzolo [18] developed an analytical model and experimental test to study the nonlinear lateral vibration, which focused on the derivation of secondary moment. The angular misalignment and the load inertia caused the moment excitation. It was suggested that variations in angular misalignment are a more critical variable to investigate when studying the level of moment excitation. SoltanRezaee et al. [19, 20] studied the torsional stability of three flexible shafts connected by a pair of universal joints. The system's stability is investigated using the monodromy matrix. The effects of angular misalignment, damping, and stiffness on the system stability were numerically studied. It was found that harmonic, sub-harmonic, and combination-type resonance regions appear in different values of angular misalignment. Saurabh K. Bharti and Samantaray [21] analysed the torsional vibration of the Cardan shaft configured in angular misalignment greater than 45°. Numerical simulations revealed that higher vibration amplitude was observed when twice of input rotational speed reaches the torsional natural frequency. It was demonstrated that the amplitude of vibrations could be reduced by lowering the angular misalignments or increasing shaft torsional damping. Yao and DeSmidt [22] studied coupled torsional-lateral vibration of the driveline connected by the Cardan shaft under constant input torque. The system experiences a dynamic angular misalignment due to vertical suspension travel. Output shaft speed, lateral and torsional vibrations were observed for different values of static angular misalignments and vertical suspension damping. Again, numerical results showed that higher torsional vibration amplitude was observed when twice of input rotational speed reaches the torsional natural frequency. The torsional vibration was reported to be reduced by reducing load or increasing input torque.

Apart from studies on the effect of angular misalignment, there exists limited initial research into vibrations caused by out-of-phase position. An and Wang [23] investigated the kinematic relationship of a driveline with a Cardan shaft, including the effects of unequal angular misalignments and nonzero phase angles. Their results shown that the output shaft speed fluctuations worsen when these two conditions occur simultaneously. Fischer and Paul [24] experimentally showed that under equal angular misalignment for both joints, the fluctuation is cancelled if the phase angle is equal to the twist angle. Wu et al. [25] showed that proper phase angle arrangement in multi universal joints system could attenuate the torsional vibration and should be considered when designing a driveshaft.

The torsional and lateral vibrations caused by a combination of angular misalignment and out-of-phase position of the Cardan shaft were not thoroughly investigated in the previous study. To the best knowledge of these authors, most of the published research analyses torsional and lateral

vibrations with the in-phase position. This study presents a model for analyzing the torsional and lateral vibration of a transmission system driven by a Cardan shaft. The aim is to examine the possibility of an out-of-phase position displaced by a phase angle in attenuating the vibrations. The governing equations representing the dynamics of the system are derived. Numerical simulations are carried out for a range of angular misalignments. The steady-state vibration responses are compared for in-phase and out-of-phase positions. Relative attenuation is used to investigate the effect of the phase angle in attenuating the vibration amplitudes.

Apart from this introduction, the remainder of this study is organized as follows. Section 2.1 provides a detail on system parameters and underlying assumptions. Section 2.2 is focused on developing the mathematical model. Section 2.3 involves assigning a set of parameter values. Section 3 presents numerical simulation results for both in-phase out-of-phase positions. The effects of the phase angle on vibration attenuation are discussed. This article is concluded with viewpoints in Section 4. Figure 1 shows the flow chart of the process involves.

2.0 METHODOLOGY

2.1 System Description

The schematic representation of the power transmission system is shown in Figure 2. The Cardan shaft is assumed to be torsionally flexible and connected to rigid input and output shafts. This rotational system is configured in Z-configuration, with angular misalignment only in a single plane, the XZ-plane.
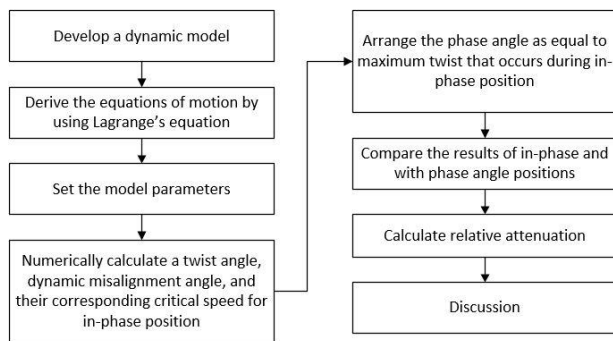
Figure 1 Flowchart of methodology

The rotor disk is attached to the end of the output shaft and mounted on a support structure that provides translational stiffness and damping property in Z-axis. It is assumed that the output shaft bending stiffness is greater than the stiffness of the support structure. So, the output shaft only experiences rigid lateral modes which cause fluctuation in angular misalignment. In-line with study by Yao and DeSmidt

[22], the present study assumed that even when subjected to lateral fluctuation, both universal joints remained in equal angular misalignment. Furthermore, the rotary inertia of the universal joints and friction effects are neglected.
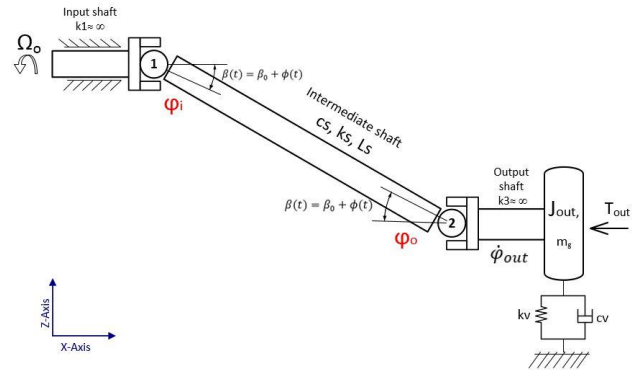
Figure 2 Schematic of transmission system dynamic model

The model parameters are described as follows. The quantity J_{out} represents the total rotary inertia of the rotor, output shaft, and any additional spinning components on the output shaft side, while m_g is the total suspended mass of the load end. T_{out} represents the constant loading torque. The quantity Ω_o and $\dot{\varphi}_{out}$ represent the input shaft's and output shaft's speed. The angular position of the yokes on the drive and driven sides of the Cardan shaft is denoted by φ_i and φ_o, respectively.

The Cardan shaft has a length of L_s and an outer diameter of d_o. The Cardan shaft's torsional stiffness is k_s, while k_v is the support structure's stiffness. Torsional viscous damping is given as $c_s = \xi_s k_s$, where ξ_s is the material's viscous damping parameter. The support structure's damping coefficient is $c_v = \xi_v k_v$, where ξ_v is the viscous damping parameter. The angular misalignment for each universal joint is represented by β. Dynamic angular misalignment, ϕ due to elastic deformation of the support, is calculated by considering the moment equation about point 1. Thus, β is due to both the static, β_0 and dynamic angular misalignment.

2.2 Equations of Motion

The model of the system is developed based on kinematic equations of a single universal joint with constant angular misalignment, β as shown in Figure 3.
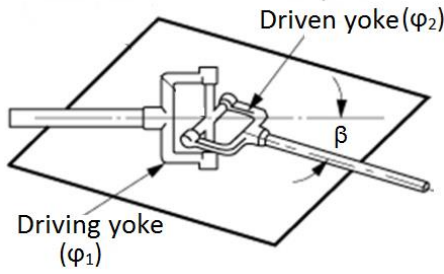
Figure 3 Single universal joint

Figure 4 Phase angle between the two universal joint yokes

The well-known kinematic relationship between the angular positions of the driving and driven yokes of a universal joint can be expressed as [26, 27].

$$tan(\varphi_2) = \frac{tan(\varphi_1 t)}{cos(\beta)} \tag{1}$$

Equation 1 shows that as angular misalignment increases, the fluctuation in angular positions of driven yokes intensifies. In Figure 2, when the driven rotor fluctuates in the lateral direction, the angular misalignment of the joint varies. Thus, the resulting time function angular misalignment, $\beta(t)$ is a combination of static, β_0 and dynamic angular misalignments, $\phi(t)$ [14].

$$\beta(t) = \beta_0 + \phi(t) \tag{2}$$

From the kinematic relationships given in Equation 1, the angular positions of the yokes on the driving and driven sides of the Cardan shaft with the presence of dynamic angular misalignments can be expressed as

$$tan(\varphi_i) = \frac{tan(\Omega_0 t)}{cos(\beta_0 + \phi)} \tag{3}$$

$$tan(\varphi_o) = \frac{tan(\varphi_{out})}{cos(\beta_0 + \phi)} \tag{4}$$

For transmission system with rigid Cardan shafts, a constant output shaft speed is guaranteed if the both angular misalignments are identical and configured with in-phase position [22, 28]. The Cardan shaft is the in-phase position when the yokes of the two universal joints are aligned in a plane. A phase angle, α is an angle between the two planes of the yokes mounted on the Cardan shaft. A nonzero phase angle indicates an out-of-phase position. In this study, the aim is to examine the possibility of an out-of-phase position displaced by a phase angle in attenuating the vibrations. So, the phase angle, α is displaced in the same direction as the input rotational motion by shifting the yoke on the driven side of Cardan shaft as shown in Figure 4.

Therefore, Equation 4 is rewritten with the presence of phase angle as

$$tan(\varphi_o - \alpha) = \frac{tan(\varphi_{out} - \delta)}{cos(\beta_o + \phi)} \tag{5}$$

where δ represents a displaced angular position of the output shaft's yoke and is calculated as [26]

$$tan(\delta) = tan(\alpha) \, cos(\beta_o) \tag{6}$$

Then, the first derivative of Equations 3 and 5 with respect to time gives the relationship of angular speed at the driving and driven ends of the Cardan shaft, which is expressed as [28]

$$\dot{\varphi}_i = \Omega_0 \frac{cos(\beta_o + \phi)}{1 - sin^2(\beta_o + \phi) \, cos^2(\Omega_0 t)} + \dot{\phi} \frac{0.5 \, sin(2\Omega_0 t) \, (sin(\beta_o + \phi))}{1 - sin^2(\beta_o + \phi) \, cos^2(2\Omega_0 t)} \tag{7}$$

$$\dot{\varphi}_o = \dot{\varphi}_{out} \frac{cos(\beta_o + \phi)}{1 - sin^2(\beta_o + \phi) \, cos^2(\varphi_{out} - \delta)} + \dot{\phi} \frac{0.5 \, sin(2\varphi_{out} - 2\alpha) \, (sin(\beta_o + \phi))}{1 - sin^2(\beta_o + \phi) \, cos^2(\varphi_{out} - \delta)} \tag{8}$$

The system equations of motion are derived by using Lagrange's equations

$$\frac{d}{dt}\left(\frac{\partial K}{\partial \dot{q}_i}\right) - \frac{\partial K}{\partial q_i} + \frac{\partial D}{\partial \dot{q}_i} + \frac{\partial P}{\partial q_i} = Q_i, i = 1,2,.,n \tag{9}$$

with the system's generalized coordinate representing rotational motion, φ_{out} and lateral motion, ϕ is described as

$$q = \{\varphi_{out} \quad \phi\}^T \tag{10}$$

The total kinetic energy is expressed as

$$K = \frac{1}{2}J_{out}\dot{\varphi}_{out}^2 + \frac{1}{2}m_g\left(L_s \, cos\,\beta_0\,\dot{\phi}\right)^2 \tag{11}$$

The total damping dissipated energy is expressed as

$$D = \frac{1}{2}c_s(\dot{\varphi}_o - \dot{\varphi}_i)^2 + \frac{1}{2}c_v\left(L_s \, cos\,\beta_0\,\dot{\phi}\right)^2 \tag{12}$$

Substitute Equations 7 and 8 into Equation 12 results in

$$D = \frac{1}{2}c_s\left[\left(\dot{\varphi}_{out}\frac{cos(\beta_o + \phi)}{1 - sin^2(\beta_o + \phi) \, cos^2(\varphi_{out} - \delta)} + \dot{\phi}\frac{0.5 \, sin(2\varphi_{out} - 2\delta) \, (sin(\beta_o + \phi))}{1 - sin^2(\beta_o + \phi) \, cos^2(\varphi_{out} - \delta)}\right) - \right. \tag{13}$$

$$\left(\Omega_0 \frac{cos(\beta_o+\phi)}{1-sin^2(\beta_o+\phi)\,cos^2(\Omega_0 t)} + \right.$$
$$\left.\phi \frac{0.5\,sin(2\Omega_0 t)\,(sin(\beta_o+\phi))}{1-sin^2(\beta_o+\phi)\,cos^2(2\Omega_0 t)}\right)\Big]^2 + \frac{1}{2}c_v\big(L_s\,cos\,\beta_0\,\phi\big)^2$$

The total potential energy is expressed as

$$P = \frac{1}{2}k_s(\varphi_o - \varphi_i)^2 + \frac{1}{2}k_v(L_s\,cos\,\beta_0\,\phi)^2 \tag{14}$$

Substitute Equations 3 and 5 into Equation (14) results in

$$P = \frac{1}{2}k_s\left(tan^{-1}\left(\frac{tan(\varphi_{out}-\delta)}{cos(\beta_o+\phi)}\right) - \alpha - \right. \tag{15}$$
$$\left. tan^{-1}\left(\frac{tan(\Omega_0 t)}{cos(\beta_o+\phi)}\right)\right)^2 + \frac{1}{2}k_v(L_s\,cos\,\beta_0\,\phi)^2$$

Then, the following equations of motion are obtained by substituting Equation 11,13 and 15 into Equation 9 [14]. After some arrangement, the rotational motion is expressed as

$$J_{out}\ddot{\varphi}_{out} + c_s\eta_2(\eta_2\dot{\varphi}_{out} - \eta_1\Omega_0) + k_s\eta_2(\varphi_o - \tag{16}$$
$$\varphi_i) = T_{out} - c_s\eta_2\dot{\phi}(\eta_{2A} - \eta_{1A})$$

And for lateral motion

$$m_g(L_s\,cos\,\beta_0)^2\ddot{\phi} + c_v(L_s\,cos\,\beta_0)^2\dot{\phi} + \tag{17}$$
$$[k_v(L_s\,cos\,\beta_0)^2\phi] + c_s\dot{\phi}(\eta_{2A} - \eta_{1A})^2 = -c_s(\eta_{2A} - \eta_{1A})(\eta_2\dot{\varphi}_{out} - \eta_1\Omega_0) - k_s(\varphi_o - \varphi_i)(\eta_{2A} - \eta_{1A})$$

Meanwhile, an angle of twist is the consequence of the angular deformation between two points placed on the Cardan shaft's opposite ends and given as [29]

$$\theta_s = \varphi_o - \varphi_i \tag{18}$$

Differentiating Equation 18 with respect to time yields [21]

$$\dot{\theta}_s = (\eta_2\dot{\varphi}_{out} - \eta_1\Omega_0) + \dot{\phi}(\eta_{2A} - \eta_{1A}) \tag{19}$$

where

$$\eta_1 = \frac{cos(\beta_o+\phi)}{1-sin^2(\beta_o+\phi)\,cos^2(\Omega_0 t)}$$
$$\eta_2 = \frac{cos(\beta_o+\phi)}{1-sin^2(\beta_o+\phi)\,cos^2(\varphi_{out}-\delta)}$$
$$\eta_{1A} = \frac{0.5\,sin(2\Omega_0 t)\,(sin(\beta_o+\phi))}{1-sin^2(\beta_o+\phi)\,cos^2(2\Omega_0 t)}$$
$$\eta_{2A} = \frac{0.5\,sin(2\varphi_{out}-2\delta)\,(sin(\beta_o+\phi))}{1-sin^2(\beta_o+\phi)\,cos^2(\varphi_{out}-\delta)} \tag{20}$$

2.3 Numerical Method and Model Parameters

Table 1 contains a representative set of parameter values chosen for this study. Assuming all shafts are perfectly aligned, which is $\beta_o = 0$, the system's natural frequencies can be calculated as $\omega_t = \left(\frac{k_s}{J_{out}}\right)^{\frac{1}{2}}$ and $\omega_l = \left(\frac{k_v}{m_g}\right)^{\frac{1}{2}}$. Based on the given data, the natural

frequency of torsional and lateral vibrations is 143 rad/s and 80 rad/s, respectively.

Table 1 Parameter values of the power transmission system

Parameters Description	Symbol	Value	Unit
Rotational inertia of the driven side	J_{out}	0.0045	kg.m²
Suspended mass	m_g	4.09	kg
Cardan shaft outer diameter	d_o	0.010	m
Cardan shaft length	L_s	0.325	m
Cardan shaft torsional stiffness	k_s	92.20	Nm.rad⁻¹
Cardan shaft material's viscous damping coefficient	ξ_s	0.002	s
Load torque	T_{out}	5	Nm
Support structures stiffness	k_v	26331	N.m⁻¹
Support structures viscous damping coefficient	ξ_v	0.002	s

Equations 16, 17 and 19 are arranged into a system of three first-order ordinary differential equations for numerical simulations.

$$\dot{X}_1 = X_2$$
$$\dot{X}_2 = [T_{out} - c_s\eta_{2X}X_4(\eta_{2AX} - \eta_{1AX}) - c_s\eta_{2X}(\eta_{2X}X_2 - \eta_{1X}\Omega_0) - k_s\eta_{2X}X_5]/J_{out}$$
$$\dot{X}_3 = X_4$$
$$\dot{X}_4 = -[c_s(\eta_{2AX} - \eta_{1AX})(\eta_{2X}X_2 - \eta_{1X}\Omega_0) - k_s(X_5)(\eta_{2AX} - \eta_{1AX}) - c_v(L_s\,cos\,\beta_0)^2X_4 - k_v(L_s\,cos\,\beta_0)^2X_3 - c_sX_4(\eta_{2AX} - \eta_{1AX})^2]/ m_g(L_s\,cos\,\beta_0)^2$$
$$\dot{X}_5 = (\eta_{2X}X_2 - \eta_{1X}\Omega_0) + X_4(\eta_{2AX} - \eta_{1AX}) \tag{21}$$

where

$$[X_1 \quad X_2 \quad X_3 \quad X_4 \quad X_5]^T = [\varphi_{out} \quad \dot{\varphi}_{out} \quad \phi \quad \dot{\phi} \quad \theta_s]^T$$
$$\eta_{1X} = \frac{cos(\beta_o+X_3)}{1-sin^2(\beta_o+X_3)\,cos^2(\Omega_0 t)}$$
$$\eta_{2X} = \frac{cos(\beta_o+X_3)}{1-sin^2(\beta_o+X_3)\,cos^2(X_1-\delta)}$$
$$\eta_{1AX} = \frac{0.5\,sin(2\Omega_0 t)\,(sin(\beta_o+X_3))}{1-sin^2(\beta_o+X_3)\,cos^2(2\Omega_0 t)}$$
$$\eta_{2AX} = \frac{0.5\,sin(2X_1-2\delta)\,(sin(\beta_o+X_3))}{1-sin^2(\beta_o+X_3)\,cos^2(X_1-\delta)} \tag{22}$$

Equation 21 is solved numerically by applying the Runge-Kutta algorithm in MATLAB. The maximum and minimum values of the responses are calculated for each input rotational speed, which ranges from Ω_o= 100 to 1500 rpm. Numerical simulations are carried out for static angular misalignments ranging from 5° to 25°. The simulation is started with an in-phase position. A critical speed is indicated by significant increases in vibration amplitude. Then, the maximum twist at critical speed is used to rearrange the phase angle. An attenuation percentage of the vibrations due to

the phase angle effects is investigated using a relative attenuation, ϵ. The relative attenuation is defined as

$$\epsilon = \frac{1}{N}\sum_{i=1}^{N}\left(\frac{A_{O,i}-A_{P,i}}{A_{O,i}}\right) \times 100\% \qquad (23)$$

where $A_{O,i}$, and $A_{P,i}$ are the maximum amplitudes of the in-phase and out-of-phase positions, respectively. N is the number of input rotational speeds.

3.0 RESULTS AND DISCUSSION

3.1 Vibration Responses of the In-Phase Position

To study torsional and lateral vibrations, the response of the transmission system is numerically calculated using Equation 21. The derived equations of motion include the value of the phase angle. In this section, the torsional and lateral vibrations of the in-phase position are studied first. Figure 5 shows the time domain of the steady-state responses for the $\beta_o = 15°$ and $\Omega_0 = 600\,rpm$. The maximum twist is 3.667° while the maximum dynamic angular misalignment is 13.4 x 10-3 °. Both torsional and lateral vibrations are periodic and dominated by a frequency component of twice the input rotational speed or second-order component, 1200 rpm or 20 Hz, as shown in Figure 6. In addition, there is a small peak of the fourth-order component at 24 Hz. Previous researches [14, 17, 25] have shown that when the angular misalignment is less than 30°, second-order vibration has a significant effect on vibration responses than fourth-order vibration. Furthermore, the approximation of the universal joint's kinematic relationship given in Equation 1 by using Taylor- McLaurin series up to second-order terms while ignoring the higher order terms is feasible[19, 30]. For this reason, the amplitude of second-order vibration is selected to characterize the dynamics of the system.Figure **7** shows the vibration responses as the input rotational speed varies for a static angular misalignment of 15°. A significant increase in torsional and lateral vibration amplitudes is observed when the input rotational speed is close to 684 rpm and 381 rpm, respectively. The vibration amplitudes have reached a peak value of 3.86° of twist and 10.2 x 10-3 ° of dynamic misalignment angle. The system suffers a resonance because the frequency of the second-order excitation brought on by the universal joint coincides with the torsional and lateral natural frequencies of the system, which are 143 rad/s (1368 rpm) and 80 rad/s (762 rpm).
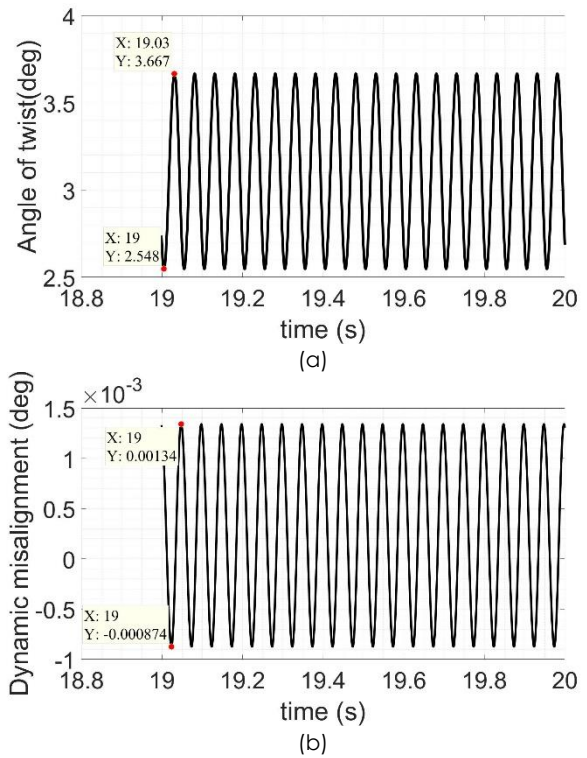
Figure 5 Time domain response at $\beta_o = 15°$ and $\Omega_0 = 600\,rpm$: (a) torsional vibration and (b) lateral vibration
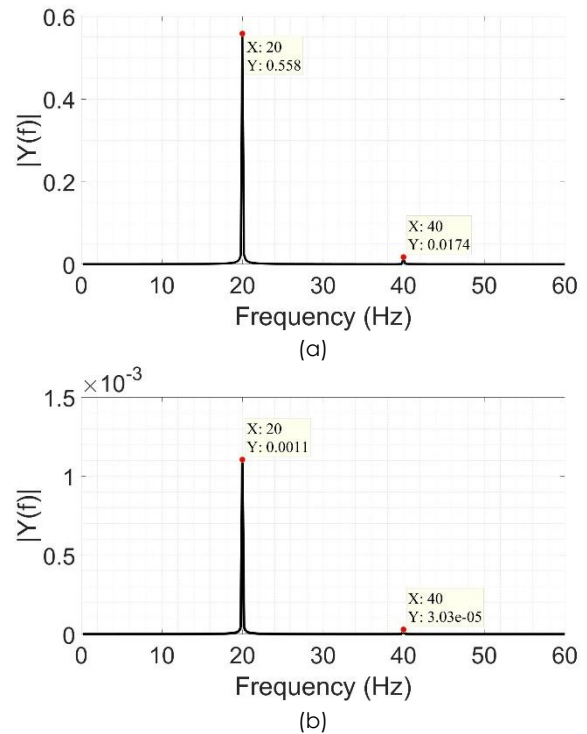
Figure 6 Frequency domain response at $\beta_o = 15°$ and $\Omega_0 = 600\,rpm$: (a) torsional vibration and (b) lateral vibration

(a)

(b)
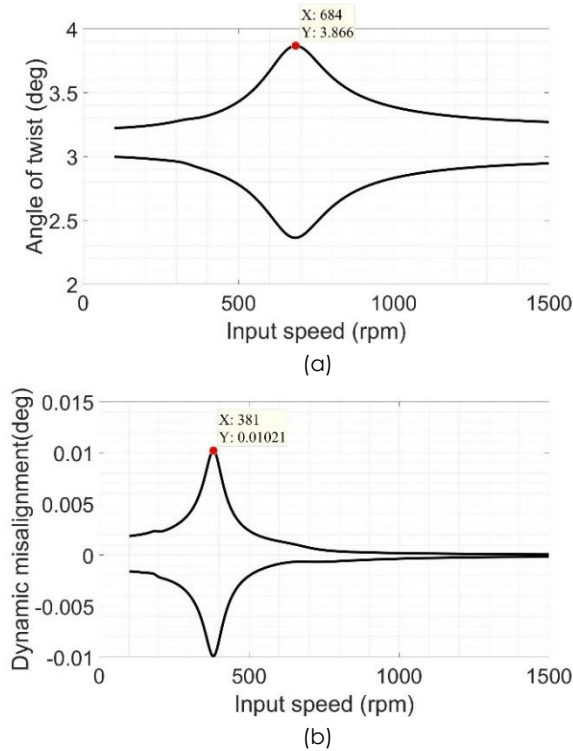
Figure 7 Variation of the steady-state responses at $\beta_o = 15°$: (a) torsional vibration and (b) lateral vibration

A numerical study was carried out in the range of 5° to 25° to investigate the effects of static angular misalignment. Table 2 depicts the maximum vibration amplitudes for five different values of static angular misalignments. From Equation 1, the vibration amplitudes are proportional to the angular misalignment of the universal joint. It is worth noting that as the static angular misalignment increases, so do the amplitudes of both torsional and lateral vibration [13, 22].

Table 2 Maximum amplitude of the steady-state response for the in-phase position

Static angular misalignment	Torsional		Lateral	
	Critical speed (rpm)	Maximum twist (deg)	Critical speed (rpm)	Maximum dynamic angle (10⁻³ deg)
5°	684	3.19	381	3.08
10°	684	3.44	381	6.39
15°	684	3.87	381	10.22
20°	684	4.48	381	14.96
25°	684	5.29	381	21.29

3.2 Vibration Responses of the Out-of-Phase Position

In attenuating the vibrations, the phase angle, α is arranged as equal to the maximum twist that occurs during the in-phase position. The displaced angular position of the output shaft's yoke, δ is calculated using Equation 6 and given in Table 3.

Table 3 Phase angle and angular position of the output shaft's yoke

Static angular misalignment	α (deg)	δ (deg)
5°	3.19	3.1
10°	3.44	3.3
15°	3.87	3.7
20°	4.47	4.2
25°	5.29	4.7

Figure 8 to Figure 12 compares the vibration responses between in-phase and out-of-phase positions. The solid line represents the in-phase position, while the dotted line represents the out-of-phase position. The torsional and lateral vibrations were significantly attenuated for all considered angular misalignments, especially at their corresponding critical speed. The figures also showed that, the existing of phase angle not alter the natural frequencies of the system at static angular misalignment lower than 25°. Therefore, the system is able to maintain the natural frequencies within the designed range.
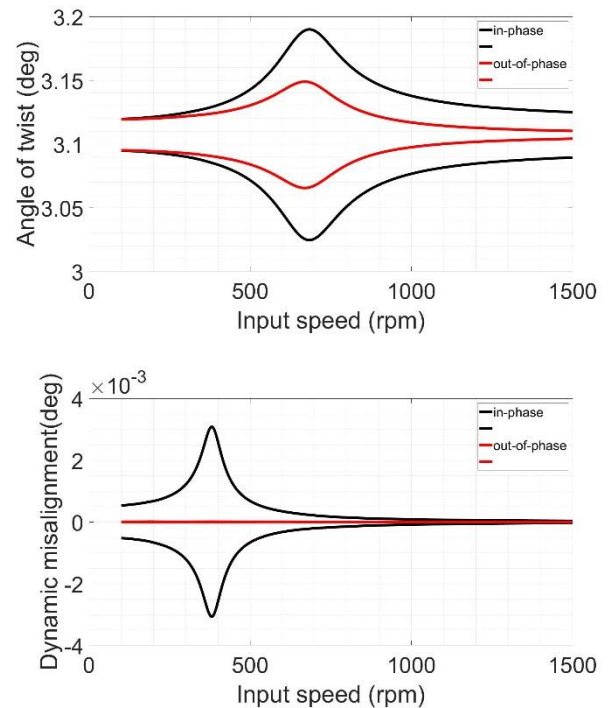
Figure 8 Comparison between in-phase and out-of-phase positions at $\beta_o = 5°$: (a) torsional vibration and (b) lateral vibration
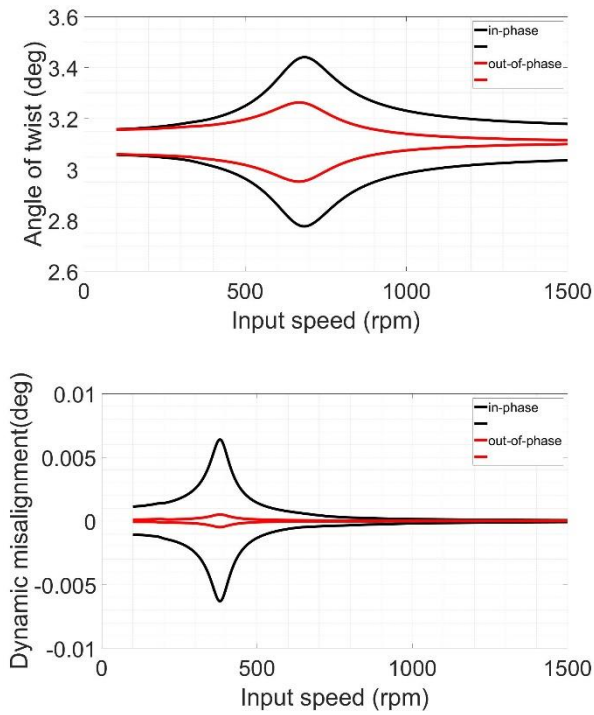
Figure 9 Comparison between in-phase and out-of-phase positions at $\beta_o = 10°$: (a) torsional vibration and (b) lateral vibration
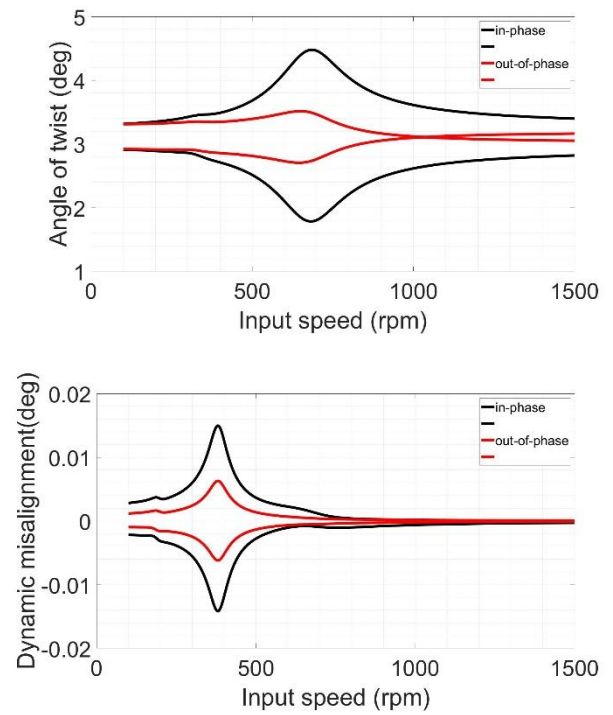
Figure 11 Comparison between in-phase and out-of-phase positions at $\beta_o = 20°$: (a) torsional vibration and (b) lateral vibration
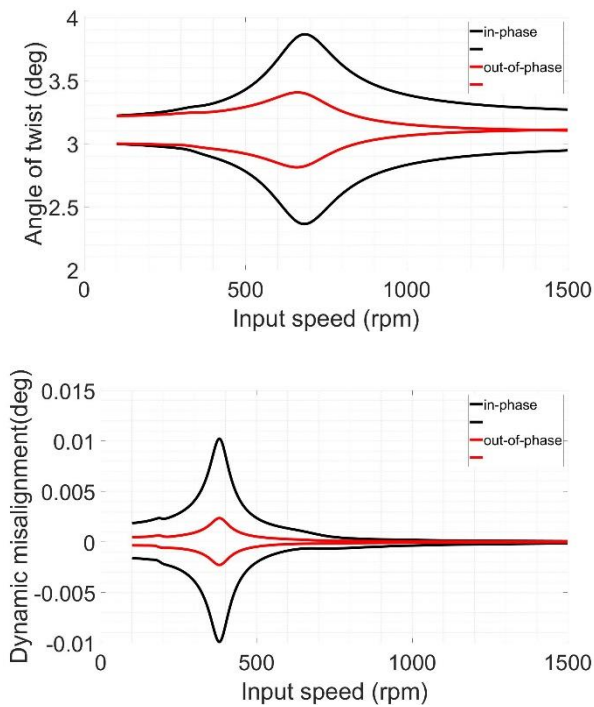
Figure 10 Comparison between in-phase and out-of-phase positions at $\beta_o = 15°$: (a) torsional vibration and (b) lateral vibration
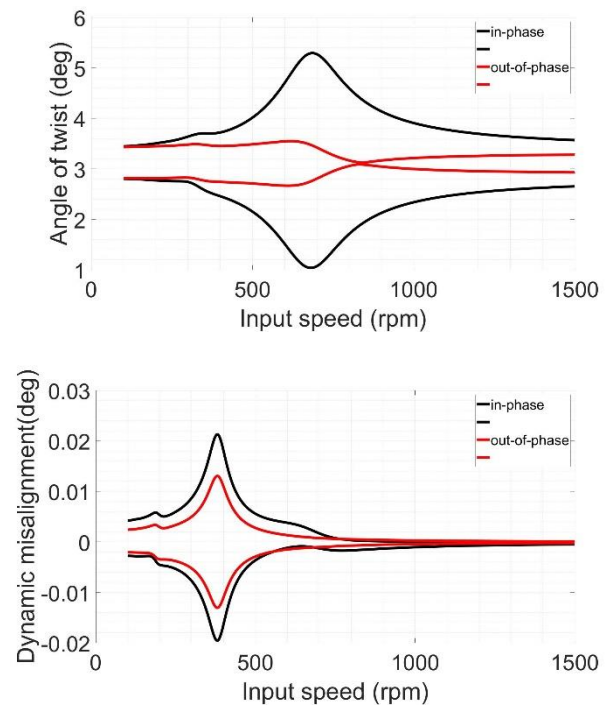
Figure 12 Comparison between in-phase and out-of-phase positions at $\beta_o = 25°$: (a) torsional vibration and (b) lateral vibration

Relative attenuation is calculated to further demonstrate the phase angle's effects in attenuating vibrations. Figure 13 shows the calculated relative attenuation for all considered values of static angular misalignments. The red line represents the torsional vibration, while the blue line represents the lateral vibration. The figure shows that as the static angular misalignment angle increases, the relative attenuation increases for torsional vibration and decreases for lateral vibration. It can be seen that for a static angular misalignment angle of less than 15°, the effect of the phase angle on the twist was not too significant. However, at a large static angular misalignment of more than 20°, the phase angle attenuated the torsional vibration by more than 10 percent. For lateral vibration, the phase angle almost eliminated the lateral vibration at static angular misalignment of less than 20°. Even though there is a decreasing trend of relative attenuation, the lateral vibration was significantly attenuated for static angular misalignment greater than 20°. It is proved that a proper phase angle arrangement can attenuate the torsional and lateral vibrations of the transmission system.
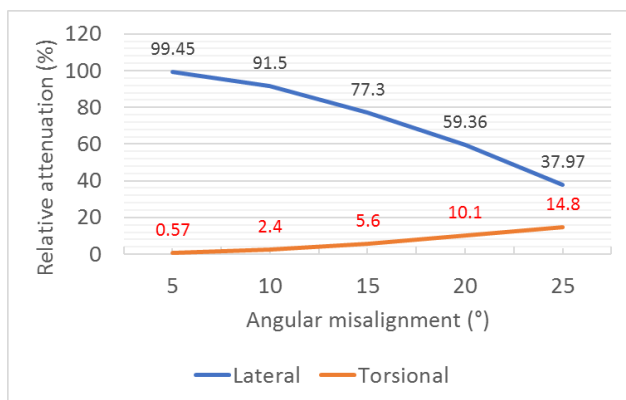
Figure 13 The relative attenuation at different values of static angular misalignments

4.0 CONCLUSION

This article studies the torsional and lateral vibrations of a transmission system employing a Cardan shaft under the effects of a nonzero phase angle. The model and analysis developed in this study incorporates the torsional damping effect into the governing equation of lateral vibration as well as the full kinematics relationship of the universal joint. The phase angle was defined as the angle between the two planes of the universal joint yokes mounted on the Cardan shaft. This study utilized the phase angle to attenuate the system's torsional and lateral vibrations. Numerical simulations were carried out for static angular misalignments up to 25 degrees. The torsional and lateral vibrations were indicated by the angle of twist and dynamic angular misalignment, respectively. The results showed that for static angular misalignment greater than 20 degrees, the proposed phase angle

arrangement could attenuate torsional vibration by more than 10 percent while significantly reducing lateral vibration. Therefore, the phase angle must be taken into account when designing a transmission system. These quantities become more important with larger static angular misalignment. The findings presented in this study may contribute in improving understanding of how phase angle arrangement affect both torsional and lateral vibrations in power transmission system employing cardan shaft. This is the motivation for future study to validate with experimental work before applying in real rotating machinery.

Conflicts of Interest

The author(s) declare(s) that there is no conflict of interest regarding the publication of this paper.

Acknowledgement

References

[1]   Bulut, G. 2014. Dynamic Stability Analysis of Torsional Vibrations of a Shaft System Connected by a Hookes Joint through a Continuous System Model. *Journal of Sound and Vibration* 333: 3691-3701.

[2]   Ding, J. M., Lin, J. H., He, L., Zhao, J. 2015. Dynamic Unbalance Detection of Cardan Shaft in High-speed Train Based on EMD-SVD-NHT. *Journal of Central South University.* 22: 2149-2157.

[3]   Zheng, Z., Lin, J., Hu, Y., Zhou, Q., Yi, C. 2022. Dynamic Unbalance Identification and Quantitative Diagnosis of Cardan Shaft in High-speed Train based on Improved TQWT-RBFNN-NSGA-II Method. *Eng Fail Anal.* https://doi.org/10.1016/j.engfailanal.2022.106226.

[4]   Golafshan, R., Dascaliuc, C., Jacobs, G., Roth, D., Berroth, J., Neumann, S. 2021. Damage Diagnosis of Cardan Shafts in Mobile Mining Machines using Vibration Analysis. *IOP Conference Series: Materials Science and Engineering.* 1097: 012019.

[5]   Porat I. 1980. Moment Transmission by a Universal Joint. *Mechanism and Machine Theory.* 15: 245-254.

[6]   Hu, Y., Zhang, B., Tan, A. C. 2020. Acceleration Signal with DTCWPT and Novel Optimize SNR Index for Diagnosis of Misaligned Cardan Shaft in High-speed Train. *Mechanical Systems and Signal Processing.* 140: 106723.

[7]   Hu, Y., Chit Tan, A., Liang, C., Li, Y. 2021. Failure Analysis of Fractured Motor Bolts in High-speed Train Due to Cardan Shaft Misalignment. *Engineering Failure Analysis.* 122: 105246.

[8]   Hu, Y., Lint, J., Tan, A. C. 2019. Failure Analysis of Gearbox in CRH High-speed Train. *Engineering Failure Analysis.* 105: 110-126.

[9]   Bulut, G., Parlar, Z. 2011. Dynamic Stability of a Shaft System Connected through a Hooke's Joint. *Mechanism and Machine Theory.* 46:1689-1695.

[10]   Asokanthan, S. F., Wang, X. H. 1996. Characterization of Torsional Instabilities in a Hooke's Joint Driven System via

Maximal Lyapunov Exponents. *Journal of Sound and Vibration*. 194: 83-91.

[11] Iwatsubo, T., Saigo, M. 1984. Transverse Vibration of a Rotor System Driven by a Cardan Joint.

[12] Ota, H., Kato, M., Sugita, H. 1985. Lateral Vibrations of a Rotating Shaft Driven by a Universal Joint: 2nd Report, Analyses and Experiments on Even Multiple Vibrations by Secondary Moment. *Bulletin of JSME*. 28: 1749-1755.

[13] DeSmidt, H. A., Wang, K. W., Smith, E. C. 2002. Coupled Torsion-lateral Stability of a Shaft-disk System Driven Through a Universal Joint. *Journal of Applied Mechanics*. 69: 261-273.

[14] Xia, Y., Pang, J., Yang, L., Zhao, Q., Yang, X. 2019. Nonlinear Numerical and Experimental Study on the Second-order Torsional and Lateral Vibration of Driveline System Connected by Cardan Joint. *JVC/Journal of Vibration and Control*. https://doi.org/10.1177/1077546319889846.

[15] Xia, Y., Pang, J., Zhou, C., Li, H., Li, W. 2015. Study on the Bending Vibration of a Two-piece Propeller Shaft for 4WD Driveline. *SAE Technical Papers*. https://doi.org/10.4271/2015-01-2174.

[16] Tchomeni, B. X., Alugongo, A. A., Masu, L. 2019. Modeling and Vibration Analysis of Twin-rotor System Interconnected by a Hooke's Joint (Part a). *Vibroengineering Procedia. JVE International*. 1-6.

[17] Tchomeni, B. X., Alugongo, A. 2020. Theoretical and Experimental Analysis of an Unbalanced and Cracked Cardan Shaft in the Vicinity of the Critical Speed. *Mathematical Models in Engineering*. 6: 34-49.

[18] Browne, M., Palazzolo, A. 2009. Super Harmonic Nonlinear Lateral Vibrations of a Segmented Driveline Incorporating a Tuned Damper Excited by Non-constant Velocity Joints. *Journal of Sound and Vibration*. 323: 334-351.

[19] SoltanRezaee, M., Ghazavi, M. R., Najafi, A., Rahmanian, S. 2018. Stability of a Multi-body Driveshaft System Excited through U-joints. *Meccanica*. 53: 1167-1183.

[20] SoltanRezaee, M., Ghazavi, M. R., Najafi, A. 2018. Parametric Resonances for Torsional Vibration of Excited Rotating Machineries with Nonconstant Velocity Joints. *JVC/Journal of Vibration and Control*. 24: 3262-3277.

[21] Bharti, S. K., Samantaray, A. K. 2021. Resonant Capture and Sommerfeld Effect Due to Torsional Vibrations in a Double Cardan Joint Driveline. *Communications in Nonlinear Science and Numerical Simulation*. 97: 105728.

[22] Yao, W., DeSmidt, H. 2021. Nonlinear Coupled Torsion/Lateral Vibration and Sommerfeld Behavior in a Double U-Joint Driveshaft. *Journal of Vibration and Acoustics*. 143: 1-15.

[23] An, K., Wang, W. 2017. Transmission Performance and Fault Analysis of a Vehicle Universal Joint. *Advances in Mechanical Engineering*. https://doi.org/10.1177/1687814017707478.

[24] Fischer, I. S., Paul, R. N. 1991. Kinematic Displacement Analysis of a Double-cardan-joint Driveline. *Journal of Mechanical Design, Transactions of the ASME*. 113: 263-271.

[25] Wu, G., Shi, W., Chen, Z. 2013. The Effect of Multi-universal Coupling Phase on Torsional Vibration of Drive Shaft and Vibration of Vehicle. *SAE Technical Paper*.

[26] Schmelz, F., Seherr-Thoss, CH-C., Aucktor, E. 1992. Universal Joints and Driveshafts. Universal Joints and Driveshafts. https://doi.org/10.1007/978-3-662-02746-2.

[27] Zajì̃ Cek, M., Dupal, J. 2014. Analytic Solution of Simplified Cardan's Shaft Model. *Applied and Computational Mechanics*. 8(2014): 215-228.

[28] Chaban, A., Łukasik, Z., Popenda, A., Szafraniec, A. 2021. Mathematical Modelling of Transient Processes in an Asynchronous Drive with a Long Shaft Including Cardan Joints. *Energies (Basel)*. https://doi.org/10.3390/en14185692.

[29] Murawski, L., Dereszewski, M. 2020. Theoretical and Practical Backgrounds of Monitoring System Of Ship Power Transmission Systems' Torsional Vibration. *Journal of Marine Science and Technology (Japan)*. 25: 272-284.

[30] SoltanRezaee, M., Ghazavi, M. R., Najafi, A., Liao, W. H. 2019. Modeling and Analysis of Rotary Mechanical Systems Linked through a U-joint. *International Journal of Mechanical Engineering and Robotics Research*. 8: 459-465.